Green Chemistry

PAPER

View Article Online
View Journal | View Issue

Cite this: *Green Chem.*, 2022, **24**, 5800

Halometallate ionic liquids: thermal properties, decomposition pathways, and life cycle considerations†

Coby J. Clarke, *[a,b] Husain Baaqel,[a] Richard P. Matthews,[a] Yiyan Chen,[a] Kevin R. J. Lovelock,[c] Jason P. Hallett[a] and Peter Licence[b]

Received 25th May 2022,
Accepted 6th July 2022

DOI: 10.1039/d2gc01983c

rsc.li/greenchem

Halometallate ionic liquids provide new opportunities for industrial catalytic processes because of their unique blend of physical and chemical properties. Tunability underpins the success of ionic liquids because small structural changes can have drastic effects on either property. Catalysis can be optimised by adjusting structures to target properties such as Lewis basicity and acidity, but the structural changes have simultaneous impacts on physical properties. In this work, we provide a thorough, methodical, and reliable list of thermal parameters to help define temperature limits to prevent catalyst poisoning and limit the need to replace costly and environmentally demanding solvents. Mechanistic insights show that decomposition is particularly detrimental for halometallate ionic liquids, and life cycle analysis highlights that lower levels of organic cations are better for economic and environmental sustainability.

1. Introduction

Ionic liquids (ILs) can dissolve large amounts of metals while retaining the free-flowing properties of liquids. The resulting metal ionic liquids are known to be highly tuneable as speciation of the metal can be controlled by the concentration of the metal, the identity of the anions, and the identity of the cations.[1] Catalysis is by far the most popular application of ionic liquids currently being adopted by industry,[2] in part because of excellent tunability of metal centres, but also because the properties of the ionic liquid medium opens up new avenues for novel and established catalysts. Examples of beneficial properties include: low vapour pressures which eliminate solvent loss and enable gas/liquid phase processes, diverse structures that improve separations, and high chemical and thermal stabilities which reduce decomposition of the liquid phase and provides access to conditions unsuitable for traditional molecular solvents.[3] However, not all ionic liquids are equal because of the vast diversity in their chemical structures, which is why studying and understanding ionic liquid physical properties is key to their success. Furthermore, altering part of an ionic liquid structure to achieve a specific task can have subsequent effects on other physical or chemical properties, making design a difficult process and further warranting the study of properties critical to industrial processes.[4]

Thermal stability is a particularly important property for halometallate ionic liquids because exceeding the upper temperature limit produces decomposition products that can poison catalysts, react with reagents and products, and change the physical properties of the medium. Degraded solvents also need to be replaced or replenished, which adds a further environmental burden because ionic liquid production involves many steps, each with energy requirements and emissions of their own.[5] Recycling is often suggested as a way to offset the environmental burden of ionic liquids, but reuse depends on preventing decomposition to maintain the performance of the catalysts – waste prevention often being the leading principle of green chemistry. These issues are especially pertinent in industrial settings, where scales are larger and prolonged lifetimes make ionic liquids more economically feasible. Furthermore, highly corrosive and harmful decomposition products (such as HF) can evolve from overheated ionic liquids, which adds a serious safety concern and provides further justification for studying decomposition pathways.[6,7]

Many emerging applications of ionic liquids exploit the unique interactions between cations, anions, and metals centres. For example, new inorganic Zn nanomaterials can be prepared directly from metallic Zn using highly coordinating ionic liquids to give a more cost-effective and environmentally

[a]Department of Chemical Engineering, Imperial College London, London, UK. E-mail: coby.clarke@nottingham.ac.uk
[b]School of Chemistry, The University of Nottingham, Nottingham, UK
[c]Department of Chemistry, University of Reading, Reading, UK

†Electronic supplementary information (ESI) available: Synthesis and characterisation, thermal analysis data, supporting NMR and MS data, DFT and LCA data. See DOI: https://doi.org/10.1039/d2gc01983c

friendly production process, a type of "controlled corrosion".[8] Novel soft materials can also be prepared directly from Lewis acidic metal ionic liquids, which are able to influence polymer architectures to provide highly flexible gels with unique surface compositions.[9] Both examples utilise opposite ends of a donating/accepting scale but intermediate properties can be accessed by design. Halozincate-based ionic liquids are of particular interest in this work because they are air and moisture stable, speciation is well known,[10] and the Lewis basicity/acidity can be controlled by changing the ratio of the organic ionic liquid and metal salt. For example, mixing $[C_nC_1Im]Cl$ and $ZnCl_2$ at a ratio of 2 : 1 gives the tetrachlorozincate(II) anion $[ZnCl_4]^{2-}$, but with each successive addition of $ZnCl_2$ polyanionic species grow as linear chains (Fig. 1),[11] which subsequently increases the Lewis acidity of the metal centres.[12] These and other halometallate systems have previously been quantified in terms of Lewis acidity through Gutmann acceptor numbers (ANs)[10,13,14] and photoelectron spectroscopy.[15] Some studies have also started to report thermophysical properties such as viscosity, but a systematic/methodical analysis of thermal properties is absent from the published literature.

Here, MX_2 (where M = Zn and X = Cl^- or Br^-) was dissolved in ionic liquids with identical or mixed anions to give $[C_nC_1Im]X_\chi MX_2$, where the mole fraction (χ) was varied between 0–1. Other metal centres (Co, Ni, Pt, Ag) were also studied for χ = 0.33 (*i.e.*, one third of the solution was MX_2 Or AgX) to understand how thermal properties change as a function of the metal. We present a particular focus on high temperature stability because many new applications utilise elevated temperatures for catalytic processes or material applications (*e.g.*, 150–250 °C).[16–20] We also report solid–liquid transitions, which are important because they present a lower temperature limit, and together with thermal stability, define an operating range for the liquid medium. We report other industrially-relevant thermal parameters, such as long term thermal stabilities and heat capacities (C_p^o), which are used to estimate energy requirements for heating. Using hyphenated and hybridised TGA techniques and *ex situ* analysis, we also present a mechanistic insight to halometallate ionic liquid thermal decomposition and show why overheating metal containing ionic liquids is particularly detrimental, making thermal studies of metal ionic liquids a critical aspect for their adoption to industry. Finally, we present life cycle analysis (LCA) data for the production of chlorozincate ionic liquids as a function of mole fraction and discuss the environmental and economic impacts in the context of solvent and catalyst stability.

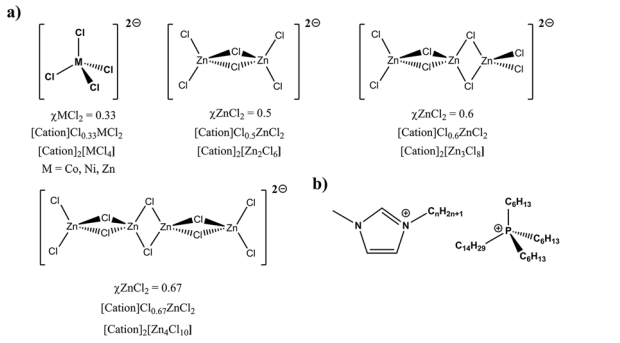

Fig. 1 Structures of (a) $[MCl_4]^{2-}$ anions and polyatomic $[Zn_xCl_{2x+2}]^{2-}$ anions with mole fractions of metals and abbreviations, (b) 1-alkyl-3-methylimidazolium and trihexyltetradecyl-phosphonium cations.

2. Experimental

2.1 General procedures

Details of synthesis and purity are presented in the ESI.† All halometallate ionic liquids prepared in this work were found to be room temperature ionic liquids (RTILs), with the exception of $[C_8C_1Im]Cl_{0.33}PtCl_2$ which was isolated as a brown solid (*note*: the $[PtCl_4]^{2-}$ anion is square planar). Although all ionic liquids were prepared under an inert atmosphere in a glovebox, the samples were momentarily exposed to air before analysis. All ionic liquids studied in this work have previously been found to be air and moisture stable from loading samples onto sample bars in air before analysing with a range of X-ray spectroscopies that show speciation is unchanged (*i.e.*, no oxidation/decomposition).[9,21–23] Any residual water absorbed from the air before thermal analysis was removed from the sample by *in situ* drying (details below).

2.2 Thermal analysis

Differential scanning calorimetry (DSC) experiments were conducted on a TA Instruments Discovery DSC2500 equipped with an RCS-90 chiller using ≈1–5 mg of sample. The DSC was calibrated before use by baseline conditioning, temperature calibration, cell constant, reversing heat capacity calibration, and MDSC calibration with indium and sapphire calibration standards. Dry nitrogen gas was used for all experiments at a flow rate of 50 mL min^{-1}, unless stated otherwise. Samples were prepared in sealed aluminium Tzero hermetic pans with pin hole lids to allow an initial drying step (120 °C for 45 min) to drive water from the samples (*i.e.*, *in situ* drying) and to erase the thermal history of the samples. Glass transition temperatures (T_g) were measured by the midpoint method at half height on heating cycles at 10 °C min^{-1}.

Heat capacities (C_p^o) were measured with the same DSC2500 instrument in sealed aluminium Tzero pans with pin hole lids with ≈15 mg of sample. The same pre-drying step (120 °C for 45 min) was used before the instrument was switched to quasi-isothermal modulated DSC (QIMDSC) mode (temperature amplitude = 1.00 °C and period = 120 s) and C_p^o values were recorded in 20 °C increments from 20 °C to 140 °C. Data was recorded at each temperature step over a 10 minutes isothermal window and the average C_p^o value was reported, along with the standard deviation as a measure of error. To assess reproducibility, three separate sample pans containing $[C_8C_1Im][NTf_2]$ were analysed and the C_p^o (25 °C) was 714.0 ± 0.8 J mol^{-1} $°C^{-1}$ and the ΔC_p^o (140–25 °C) was calculated to be 98.1 ± 1.2 J mol^{-1} $°C^{-1}$ (*note*: the error is the standard devi-

ation of the average values; for ΔC_p^o error was propagated by the square root of the sum of the squares). The low standard deviation values demonstrated that the measurements were reproducible with a low measurement error.

Thermogravimetric analysis (TGA) was measured on a TA Instruments Discovery TGA 550 with high temperature (HT) platinum pans and a gas flow rate of 50 mL min^{-1}. A two-point temperature calibration with Zn and Alumel was carried out before analysis. For organic samples, Pt pans were cleaned by heating up to 1000 °C for 1 hour in 100 mL min^{-1} air, which also ensured the TGA furnace was regularly cleaned of decomposition residues (*note*: regular exhaust cleaning is necessary for consistent sample purge rates). For metal containing samples, Pt pans were chipped free of carbon residues and submerged in 37% HCl at 60 °C and left to stir for 24–72 h before being mechanically exfoliated in a sand bath. After washing with acetone and thoroughly drying, any remaining residue was burned away using a blowtorch for 2–3 min.

TGA-mass spectrometry (TGA-MS) was measured on a TGA/DSC 1LF/UMX Mettler Toledo Instrument (Al, Zn, and In temperature calibrated) combined with a HPR20-QIC Hidden Analytical mass spectrometer. Platinum pans were used with an inert N_2 purge at 50 mL min^{-1} and samples were dried isothermally at 100 °C for 45 min before ramping at 10 °C min^{-1}. Simultaneous thermal analysis (STA) was measured on a NETZSCH Jupiter 449F5 instrument calibrated with Zn and In, and a 50 mL min^{-1} N_2 purge was used along with Pt crucibles with a heating rate of 10 °C min^{-1}.

Kinetic analysis was carried out through either the Flynn–Wall isoconversion method,[24] modulated TGA (MTGA) method,[25] or an isothermal method.[26–28] Both Flynn–Wall and MTGA employ variable heating, but MTGA uses temperature modulation in a single experiment as opposed to several separate experiments. For MTGA experiments, a modulation temperature of 5 °C and a period of 200 s were used with Hi-Res ramping at 2 °C min^{-1}, a resolution of 6.00, and sensitivity of 1.00. Activation energies (E_a) were calculated over a 20 min window centred around 10% mass loss to ensure enough cycles had passed: the average and standard deviation of the continuous E_a signals are reported. Previously, we calculated the MTGA T_d E_a of commercial $[C_2C_1Im][NTf_2]$ (127.2 ± 2.1 kJ mol^{-1}) to be only 1.7 kJ mol^{-1} lower than a published value calculated from the isothermal method (131 kJ mol^{-1}),[26] which showed that MTGA was a rapid alternative when studying ionic liquid decomposition kinetics. The Flynn–Wall and MTGA methods are both model free and assume first order kinetics, while the isothermal method assumes zero order kinetics. Because of the difficulty in identifying decomposition pathways, we have analysed several samples in this work by multiple kinetic analyses. A recent review by Xu *et al.* gives a good overview of the different isoconversional and Arrhenius kinetics analysis methods.[29]

2.3 DFT calculations

DFT calculations were carried out using the Gaussian 16 (version C.01) suite of programs.[30] Three functionals (B3LYP,[31,32] PBE[33] and TPSS[34]) combined with Grimme's-D3 dispersion correction with the Becke and Johnson damping (BJ-damping) function (hereon referred to as B3LYP-D3BJ, PBE-D3BJ and TPSS-D3BJ) were used in conjunction with the def2-TZVPP basis set to investigate the stability of several zinc chloride species.[35] The difference in results between the three tested functionals were within the error limit for DFT (~10 kJ mol^{-1}). Consequently, further calculations of transition states and those including continuum solvent environments were carried out using B3LYP-D3BJ/def2-TZVPP only.

The CPCM (conductor-like polarisable continuum model) was used to provide a generalised solvation environment.[36,37] In this work we employed DCM and 1-hexanol to provide a continuum solvent environment with dielectric constants (ε) of 8.93 and 12.51 respectively. Recently Rowe *et al.* have employed the SMD-GIL solvent model to describe the solvation environment of bismuth halometallates.[38] Structures were fully optimised under no symmetry constraints and confirmed as minima or transition states (a single imaginary frequency) using vibrational analysis. Optimisation convergence criteria were set to 10^{-9} on the density matrix and 10^{-7} on the energy matrix, and the numerical grid was improved from the default to a pruned (optimised) grid of 99 radial shells and 590 angular points per shell. Vibrational frequencies and zero-point vibrational energy corrections (ZPE) were attained using the harmonic approximation.

2.4 Life cycle analysis

In order to estimate the cost and environmental impacts of ionic liquids from a life cycle perspective, synthesis throughout their entire supply chain was considered. This included extraction of raw materials, manufacturing of intermediate chemicals, and production (*i.e.*, cradle-to-gate). For most chemicals, data was obtained from the ecoinvent 3.8 database;[39] however, for ionic liquids and some precursors, data was unavailable. For these processes, Aspen HYSYS V11 was used to model scaled-up production processes. Physical properties were obtained from published sources or estimated using semi-empirical models or the property constant estimation system (PCES) built into Aspen-HYSYS v11. Full details are provided in the ESI.†

The total annualized cost (TAC), which estimates the cost of the product over the lifetime of the plant, is used following the approach of Towler and Sinnott.[40] In short, it consists of the annualized capital expenses (CAPEX) and the annual operating expenses (OPEX), with a 10-year plant life operating 330 days (7920 hours) a year. The environmental impacts are quantified using the life cycle assessment (LCA) approach following the ISO 14040 principles and phases: (i) goal and scope, (ii) inventory analysis, (iii) impact assessment and (iv) interpretation. Here, SimaPro was used as the LCA modeling tool, and the functional unit was 1 kg of ionic liquid—production was located in Europe. The life cycle inventory (LCI), which consists of the process inputs and outputs, was obtained from both ecoinvent when available or process simulation as explained earlier for missing data. Finally, in the impact

assessment phase, these inventories were translated into environmental impacts using ReCiPe 2016 as the characterization method, which converts data to 17 environmental indicators (midpoints) such as global warming potential (GWP) and ozone depletion, and finally aggregates into three damage areas (endpoints): human health, ecosystem quality and resources.

3. Results and discussion

3.1 Thermal stability

We first decided to investigate the halozincate series of ionic liquids to explore how changing the amount of metal affected thermal properties. This was particularly important given the previously identified change in Lewis acidity across the series, which could significantly affect how cations and anions interacted with each other and decomposition products. TGA ramping experiments in an N_2 atmosphere showed that larger quantities of $ZnCl_2$ caused a considerable increase in thermal stability for the $[C_8C_1Im]Cl_\chi ZnCl_2$ ionic liquids (Fig. 2a). For example, $T_{1\%}$ and T_{onset} values increased by 159.5 °C and 170.4 °C respectively from $\chi ZnCl_2 = 0$ to 0.67. Thermal stability was effectively found to obey a sigmoidal relationship between metal free $[C_8C_1Im]Cl$ and pure $ZnCl_2$ (Fig. 2b). This observation was also supported by bromide analogues, but the increase in $T_{1\%}$ from $\chi ZnBr_2 = 0$ to 0.67 was smaller at 123.8 °C. For $[C_8C_1Im]Cl_{0.1}ZnCl_2$, the TGA thermogram showed an initial profile that matched metal-free $[C_8C_1Im]Cl$, while a small portion of the sample (<30%) mirrored the mass losses observed for $[C_8C_1Im]Cl_{0.33}ZnCl_2$. The composition of the $[C_8C_1Im]Cl_{0.1}ZnCl_2$ ionic liquid is known to be predominantly $[C_8C_1Im]Cl$ with smaller amounts of $[C_8C_1Im]_2[ZnCl_4]$.[41] Consequently, thermal parameters have captured the decomposition of the less thermally stable organic component. However, decomposition of the organic cation may affect speciation of the residual $[ZnCl_4]^{2-}$ anion—this will be discussed later in this work—so we have reported these values as an upper limit to prevent significant decomposition of the liquid phase and poisoning of the metal complex.

Halide containing ionic liquids have been demonstrated to decompose *via* reverse Menshutkin chemistry,[42] where the

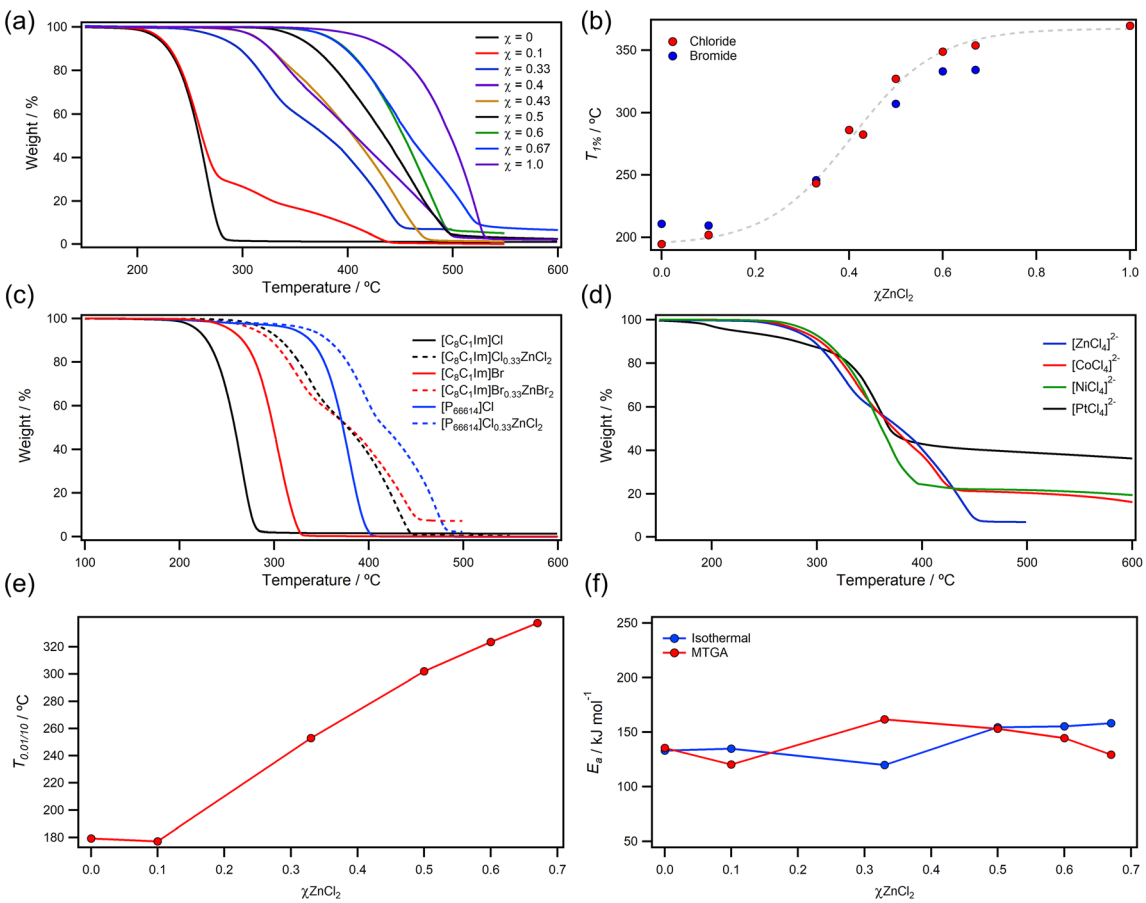

Fig. 2 TGA data and derived parameters of halometallate ionic liquids in N_2, showing: (a) 10 °C min^{-1} ramping experiments for $[C_8C_1Im]Cl_\chi ZnCl_2$; (b) plot of $T_{1\%}$ as a function of $ZnCl_2$ mole fraction for $[C_8C_1Im]Cl_\chi ZnCl_2$, with bromide analogues; (c) 10 °C min^{-1} ramping experiments for [Cation]$X_{0.33}ZnX_2$ with metal-free analogues; (d) 10 °C min^{-1} ramping experiments for $[C_8C_1Im]Cl_\chi MCl_2$ for four tetrahedral metals; (e) long term thermal stability parameter $T_{0.01/10}$ as a function of mole fraction for $[C_8C_1Im]Cl_\chi ZnCl_2$; (f) E_a of thermal decomposition for $[C_8C_1Im]Cl_\chi ZnCl_2$ from isothermal and MTGA.

halide anion acts as a nucleophile to produce neutral chloroalkanes and alkylimidazoles.[43] For $[C_8C_1Im]X_\chi ZnX_2$, thermal stability significantly increased after all free halide anions had been bonded by ZnX_2 in the $[ZnX_4]^{2-}$ complex. This suggested that the reverse Menshutkin decomposition pathway is either suppressed or regulated by the breaking of Zn–X bonds. The identity of the halide anion had very little effect on stability of $[ZnX_4]^{2-}$ imidazolium ionic liquids because $T_{1\%}$ showed a 0.1 °C difference for Cl^- *vs.* Br^- (Table 1). However, analysis of the phosphonium analogue $[P_{66614}]Cl_{0.33}ZnCl_2$, which also contains the anionic complex $[ZnCl_4]^{2-}$, showed that the stability of $[ZnCl_4]^{2-}$ could exceed the upper limit of the imidazolium analogues. Unfortunately, a large deviation between $T_{1\%}$ and T_{onset} highlighted that small amounts of weight loss were occurring at lower temperatures for $[P_{66614}]Cl_{0.33}ZnCl_2$, which was likely caused by low level haloalkane impurities from the commercially sourced ionic liquid.[44] Regardless, bulk decomposition did occur at higher temperatures (T_{onset} was 71.6 °C higher than $[C_8C_1Im]Cl_{0.33}ZnCl_2$), which indicated that steric hinderance was reducing the rate of the reverse Menshutkin process at lower temperatures (supported by the similarity of the TGA profiles) and therefore raising thermal stability.

Following analysis of the halozincate series, we next looked into the effects of different metal centres on thermal stabilities. From $T_{1\%}$ values, the order of stability was Ni > Co > Zn ≫ Pt for $[C_8C_1Im]Cl_{0.33}MCl_2$ ionic liquids. In most cases, the identity of the metal centre had very little effect on the initial decompositions of the samples. For example, there was a small 18.8 °C difference between $[C_8C_1Im]Cl_{0.33}NiCl_2$ and $[C_8C_1Im]Cl_{0.33}ZnCl_2$. However, the $[C_8C_1Im]Cl_{0.33}PtCl_2$ sample was found to undergo a series of decomposition steps from 171.7 °C, which was ≈90 °C lower than that of the $[C_8C_1Im]Cl_{0.33}NiCl_2$ ionic liquid. Unlike all other metals, the $[PtCl4]^{2-}$ complex is square planar and capable of forming large cluster $[Pt_nCl_m]^-$ anions under certain conditions.[46,47] Thermal decomposition of $[NH_4]_2[PtCl_4]$ has previously been reported and the authors have suggested that decomposition proceeds through Cl^- loss to give $[PtCl_3]^-$ which then decomposes to volatile products and involatile Pt nanoparticles.[48] Similar decomposition mechanisms have been reported for $[NH_4]_3Cl[ZnCl_4]$, which passes through the $[NH_4]_2[ZnCl_4]$ intermediate to give volatile $ZnCl_2$ and $[NH_4]Cl$.[49] One publication has also reported that heating $[C_7C_1Im][NiCl_4]$ to 700 °C for 1 hour (far beyond $T_{1\%}$ or T_{onset}) gives mixtures of $NiCl_2$ and metallic Ni.[50] Altogether, these reports suggest that M–Cl dissociation is likely to be the initial decomposition step of halometallate anions, with the potential to form larger bridged clusters as Cl^- is lost. Weakening of the Fe–Cl bonds as a function of temperature has even been observed experimentally during *in situ* XAFS measurements of $[FeCl_4]^-$ ionic liquids.[51] However, very little mechanistic insight has been presented to date. Interestingly, the difference between $T_{1\%}$ values for $[C_8C_1Im]Cl_{0.33}ZnCl_2$ and $[P_{66614}]Cl_{0.33}ZnCl_2$ observed in this work indicated the decomposition mechanism is cation dependant and thus more complex.

Long term thermal stability was evaluated using the $T_{0.01/10}$ parameter (the temperature at which 1% mass loss occurs over 10 hours) to provide more accurate upper temperature limits over extended periods (Fig. 2e and Table 1). As expected, $T_{0.01/10}$ values were consistent for metal free halide ionic liquids such as $[C_8C_1Im]Cl$ and $[C_8C_1Im]Br$, deviating by only 2.2 °C. For the $[C_8C_1Im]Cl_\chi ZnCl_2$ series, the presence of nucleophilic Cl^- anions limited stability as observed with $T_{1\%}$ data, but once all free chloride was sequestered in the $[ZnCl_4]^{2-}$ coordination complex, $T_{0.01/10}$ values significantly increased and reached a maximum at 337.5 °C for $[C_8C_1Im]Cl_{0.67}ZnCl_2$. This value is approximately 138 °C higher than ionic liquids with $[NTf_2]^-$ anions[26] and marginally exceeds the values of thermally robust dicationic ionic liquids.[27] Furthermore, the 158.3 °C increase in $T_{0.01/10}$ from metal free $[C_8C_1Im]Cl$ to metal-rich $[C_8C_1Im]Cl_{0.67}ZnCl_2$ covers a wide temperature range than spans all other published data. E_a values were within the expected ranges for ionic liquids[26] and both stepwise and MTGA derived values were reasonably similar for both techniques, but values diverged for $\chi = 0.33$. This was most likely due to a change in reaction mechanism which invalidated one of the assumptions of a zero order (stepwise) or first order (MTGA) mechanism.

Alongside high temperature thermal analysis, we have also report low temperature thermal transition and heat capacities measured using DSC (Table 1) Previous publications have reported some DSC data for halometallate ionic liquids, but large swings in melting points the presence of multiple glass transitions suggests the data was influenced by experimental factors.[10,52] We have therefore aimed to provide high quality and reliable DSC data by avoiding the use of a Glovebox, which is subject to pressure swings and therefore difficult to get accurate masses for heat capacity measurements. Instead, we have prepared samples in air using an analytical balance with pinhole pans, followed by drying procedures (see Experimental) to remove residual water from momentary exposure to air. Organic and aqueous solvents have large impacts on heat capacities,[53] so thorough drying is a necessity for accurate data. All ionic liquids (except $[C_8C_1Im]Cl_{0.33}PtCl_2$) were found to have low temperature glass transitions, and small variations in T_g values were noted for changes in composition. Using the measured T_g values from DSC and $T_{1\%}$ values from TGA, we have calculated and reported liquid ranges for most ionic liquids. The measured C_p^o values of metal free ionic liquids were in the expected ranges.[54] However, metal ionic liquids had significantly higher C_p^o values that generally increased with higher mole fractions as molecular weight increased. This highlighted that the energy requirements for heating bulk ionic liquids would be significantly higher if the metal ionic liquids were used—further justification for the drive towards thin films and solid supports.

3.2 Decomposition mechanism

After our initial TGA experiments, we were motivated to further investigate decomposition mechanisms to understand how ionic liquid structures decompose in the presence of

Table 1 Thermal parameters from temperature ramping TGA and DSC experiments at 10 °C min^{-1} (T_m, T_g, $T_{1\%}$, T_{onset})

					Thermal parameters/°C						E_a/kJ mol^{-1}				C_p^o/J mol^{-1} °C^{-1}	
Cation	Anion	Metal	χ	MW	T_m	T_g	$T_{1\%}$	T_{onset}	Liquid range	MTGA	Flynn–Wall	Isothermal	Stepwise	$T_{0.01/10}$/°C	25 °C	140–25 °C
$[C_8C_1Im]^+$	Cl^-	$ZnCl_2$	0	230.8		−59.91	194.5	238.6	254.4	135.6 ± 1.6	140.8	129.9[a]	133.1 ± 5.7	179.2	399.3 ± 0.4	64.2 ± 0.4
			0.1			−49.74	201.6	232.1	251.3	120.4 ± 0.9			134.8 ± 1.1	177.1		
			0.33	597.8		−43.55	243.3	286.8	286.9	161.1 ± 7.5	170.4		161.7 ± 4.9	252.1	780.6 ± 0.5	117.9 ± 0.5
			0.4			−43.56	286.2	309.8	329.7							
			0.43			−46.45	282.5	305.3	329.0							
			0.5	734.1		−47.35	327.0	373.8	374.3	153.2 ± 0.8			154.5/46.1	301.9	1156.1 ± 0.7	167.3 ± 0.8
			0.6	870.4		−52.81	348.9	392.8	401.7	144.7 ± 0.4			155.3 ± 4.2	323.6	1038.6 ± 0.9	118.9 ± 1.1
			0.67	1006.7		−38.39	354.0	409.0	392.4	129.3 ± 0.8	164.2		158.2 ± 4.1	337.5	1337.0 ± 0.8	154.3 ± 1.4
			1	136.3			369.8	473.5								
$[C_8C_1Im]^+$	Br^-	$ZnBr_2$	0	275.2		−64.98	208.2	277.4	273.1	121.8 ± 0.5			129.3 ± 3.2	181.4	411.2 ± 0.2	57.7 ± 0.2
			0.1			−49.68	206.8	247.6	256.5	124.7 ± 0.6						
			0.33	597.8		−44.21	243.4	300.6	287.6	152.0 ± 1.0			120.0 ± 4.6	253.0	802.6 ± 0.3	142.5 ± 0.5
			0.5	1000.8		−54.73	304.9	380.5	359.7	157.0 ± 0.2					997.9 ± 0.8	125.8 ± 0.9
			0.6	1226.0		−45.37	330.7	396.2	376.1	150.6 ± 1.3					1048.9 ± 0.6	80.9 ± 0.9
			0.67	1451.2		−35.96	332.0	401.4	368.0	140.5 ± 0.8			151.0 ± 1.2	331.3	1254.9 ± 0.7	89.4 ± 1.3
$[P_{66614}]^+$	Cl^-	$ZnCl_2$	0	519.3		−68.96	216.1	350.3	285.0	155.5 ± 2.1	118.8	114.0			1117.3 ± 0.7	184.3 ± 1.7
			0.33	1174.9		<−90	225.8	358.4	<315.8	176.1 ± 0.8	185.6		117.4 ± 2.5/32.2 ± 4.0	314.0	2337.7 ± 1.3	496.2 ± 2.2
$[C_8C_1Im]^+$	Cl^-	$NiCl_2$	0.33	591.2		−43.75	262.0	313.5	305.8	146.0 ± 0.6			143.8	244.7	866.3 ± 0.4	109.4 ± 0.5
		$CoCl_2$	0.33	591.4		−42.21	253.6	295.4	295.8	150.9 ± 0.6			116 ± 4.5/79.9 ± 6.7	231.9	875.1 ± 0.2	135.0 ± 0.4
		$InCl_3$	0.5	451.9		−47.6	351.7	422.1	399.3	138.6 ± 0.3					600.8 ± 0.4	35.8 ± 1.4
		$PtCl_2$	0.33	727.5	73.07[b]	−26.28[b]	171.7	179.5	98.6	143.8 ± 0.5						
$[C_8C_1Im]^+$	Cl^-	AgCl	0.33	604.9			211.0	236.3		133.7 ± 2.7			133.6 ± 2.6	197.2		
$[C_8C_1Im]^+$	Br^-	AgBr	0.33	738.2			232.6	265.9		127.9 ± 5.0						
$[P_{66614}]^+$		AgCl	0.33	1174.9		−71.54	208.1	329.74	279.6	151.5 ± 0.5						
$[C_4C_1Im]^+$	Cl^-	$ZnCl_2$	0	174.7		−62.73[d]	202.0	245.2	264.7	152.5 ± 1.5		132.2[a]	133.5 ± 1.3	180.7		
			0.5	621.9		−49.23	320.2	370.8	369.4	143.4 ± 1.1					732.3 ± 0.3	79.7 ± 0.6
$[C_2C_1Im]^+$	Cl^-	$ZnCl_2$	0	146.6	89.00[e]											
			0.33	429.5	97.47[c]											
			0.5	565.8	45.15[c]											
$[C_8C_1Im]^+$	Br^-	$ZnCl_2$	0.33	686.7		−43.91	247.4	279.5	291.3	147.8 ± 0.6					896.7 ± 0.6	135.5 ± 0.6
			0.5	823.0		−44.68	293.7	363.5	338.4	145.1 ± 0.5			150.6 ± 4.0/67.1 ± 2.7	282.2	1025.0 ± 0.6	128.2 ± 0.7
$[C_8C_1Im]^+$	Cl^-	$ZnBr_2$	0.5	911.9		−52.64	312.8	382.6	365.5	155.1 ± 0.3			142.5 ± 4.1/100.5 ± 1.3	295.3	1020.4 ± 0.2	132.7 ± 0.5

[a] From ref. 26. [b] T_m of amorphous solid, T_g of supercooled liquid. [c] From ref. 10. [d] T_g of supercooled liquid. [e] From ref. 45.

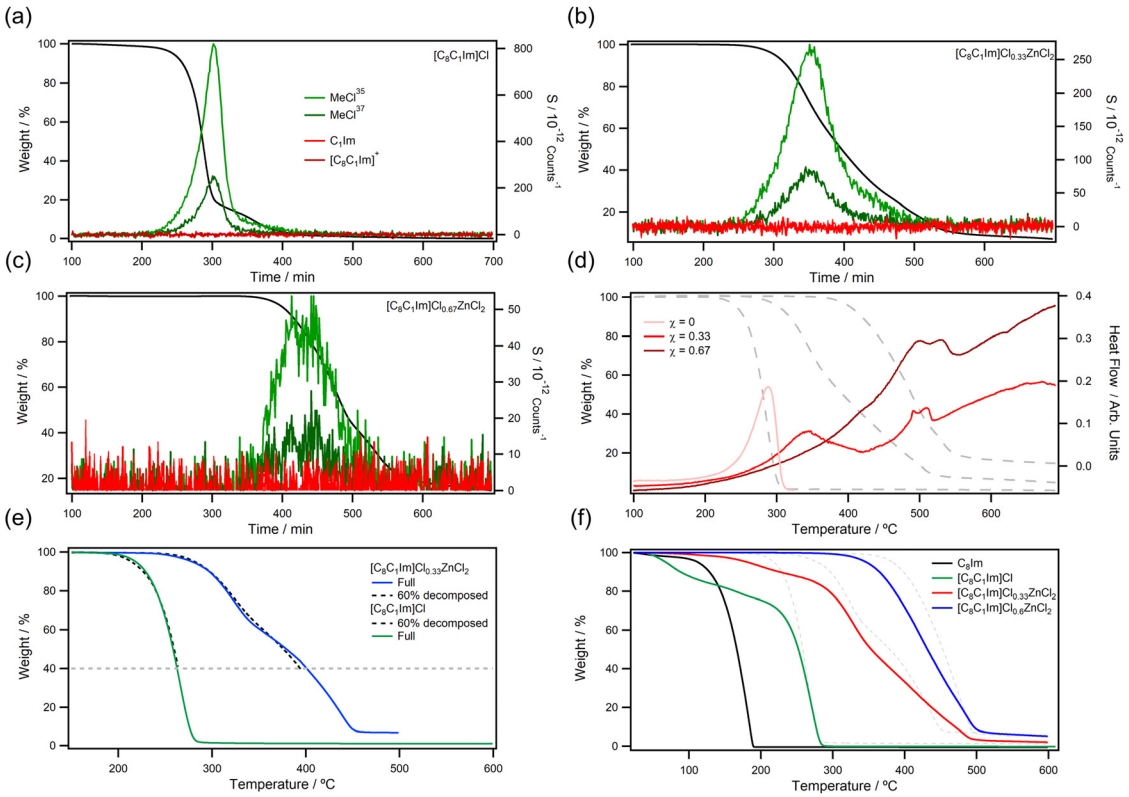

Fig. 3 (a–c) TGA-MS data for $[C_8C_1Im]Cl_\chi ZnCl_2$ where χ = 0 (a), 0.33 (b), and 0.67 (c). (d) STA data for the same $[C_8C_1Im]Cl_\chi ZnCl_2$ ionic liquids. (e) Example TGA abort thermograms for *ex situ* analysis. (f) TGA data for selected ionic liquids spiked with 15% C_8Im (coloured, solid) and the pure ionic liquids without C_8Im for comparison (grey, dashed).

metals. Insights such as this can help in the design of more robust solvents and catalysts or help to identify harmful decomposition products to improve safety on large scales. Firstly, we chose to analyse decomposition vapours of the $[C_8C_1Im]Cl_\chi ZnCl_2$ series using hyphenated TGA-MS (Fig. 3a–c). Importantly, TGA-MS favours volatile species because low volatility decomposition products can condense in transfer lines or exhaust ports. In this work, we observed mainly hydrocarbon fragments and the reverse Menshutkin product MeCl, as expected from previous reports on metal free ionic liquids.[27,55] Interestingly, $[C_8C_1Im]Cl$, $[C_8C_1Im]Cl_{0.33}ZnCl_2$, and $[C_8C_1Im]Cl_{0.67}ZnCl_2$ were all found to release MeCl on heating. This supported the hypothesis that free chloride was produced as a decomposition product in metal containing $[C_8C_1Im]Cl_\chi ZnCl_2$ ionic liquids when they were heated to high temperatures. Liberated Cl^- is expected to immediately participate in the reverse Menshutkin decomposition mechanism at high temperatures, releasing chloroalkanes and alkylimidazoles. Alkylimidazole by-products have significantly lower volatility than chloroalkanes, hence why they are not observed in TGA-MS but are observed in vacuum based thermal decomposition studies.[56] MeCl was also observed during decomposition of $[C_8C_1Im]Cl_{0.33}NiCl_2$ (ESI, Fig. S133a†), which highlighted that the same process was occurring for different metals. Unlike the imidazolium ionic liquids, $[P_{66614}]Cl_{0.33}ZnCl_2$ did not produce MeCl because it does not contain a methyl group (ESI, Fig. S133c†). Larger chloroalkanes were not observed, most likely because of low volatility and/or steric hinderance around the phosphonium centre.

STA data for $[C_8C_1Im]Cl$ showed a sharp endothermic signal during mass loss (Fig. 3d), which indicated that a single decomposition process dominated. For $[C_8C_1Im]Cl_{0.33}ZnCl_2$, the two-step decomposition gave two endothermic signals—the first signal matched that of $[C_8C_1Im]Cl$ while the second signal matched that of $[C_8C_1Im]Cl_{0.67}ZnCl_2$. Broadening of the first signal indicated that the decomposition process was not as well defined as $[C_8C_1Im]Cl$, because Zn–Cl bond dissociation was restricting the decomposition process. Interestingly, this data suggested that decomposition did proceed through reverse Menshutkin chemistry, and as volatile products vaporised, the remaining $ZnCl_2$ concentrated in the ionic liquid so that subsequent decompositions matched that of high $ZnCl_2$ content ionic liquids. This process would ultimately give $ZnCl_2$ which has a higher $T_{1\%}$ than any of the ionic liquids measured in this work. $[P_{66614}]Cl_{0.33}ZnCl_2$ also produced a similar heat flow profiles to $[C_8C_1Im]Cl_{0.33}ZnCl_2$ on thermal decomposition, but $[C_8C_1Im]Cl_{0.33}AgCl$ and $[C_8C_1Im]Cl_{0.33}NiCl_2$ gave less well defined profiles suggesting competing processes could be occurring during decomposition (ESI, Fig. S134†).

Following hybridised and hyphenated TGA techniques, we decided to analyse decomposition residues to broaden our analytical tool belt and shed insight on the involatile products that do not immediately contribute to mass loss. We programmed an abort method to stop TGA experiments at predetermined mass losses, and then analysed the residues *ex situ* with ^{1}H NMR spectroscopy (ESI, Fig. S63–69†) and +ve mode ESI-MS (Table 2 and ESI, Fig. S62†). These methods probe the organic cationic components; difficulties in analysing chlorozincate anions with techniques such as Raman (vibrational frequencies can be difficult to assign),[57] and −ve mode MS (dianions dissociate to monoanionic species)[58] make probing the inorganic component challenging. Nevertheless, the ^{1}H NMR and MS data presented in this study has proven to be very insightful for understanding decomposition mechanisms.

NMR analysis of the TGA pan residue after 60% thermal decomposition of $[C_8C_1Im]Cl$ primarily showed the presence of four compounds (ESI, Fig. S63†) which were identified by high-resolution mass spectrometry as the intact $[C_8C_1Im]^+$ cation (*m/z* 195), the mixed alkyl chain products $[C_1C_1Im]^+$ (*m/z* 97) and $[C_8C_8Im]^+$ (*m/z* 293), and neutral *N*-octylimidazole C_8Im. For the latter, the protonated product was identified in MS (*m/z* 181; ESI, Fig. S62†), but the molecule was confirmed to be neutral by comparing the ^{1}H NMR chemical shifts with those of synthesised C_8Im (ESI, Fig. S63 and S65†) and HC_8Im (ESI, Fig. S66†). The intact $[C_8C_1Im]^+$ cation was the major component of the residue (Table 2) with the decomposition products present in smaller amounts (generally <15%), but the quantities depended upon the degree of thermal decomposition. Presence of the mixed chain products suggested that neutral decomposition products C_nIm and C_nCl were reacting in the ionic liquid phase to form new ionic liquid cations—which is also indirect evidence of the reverse Menshutkin mechanism. Analysis of decomposed $[C_8C_1Im]Cl_{0.33}ZnCl_2$ (ESI, Fig. S67–69†) and the bromide analogue showed that the exact same decomposition products were produced, but larger quantities of neutral C_8Im were present, along with neutral C_1Im (*m/z* 83; protonated salt). The same result was also found for $[C_8C_1Im]Cl_{0.6}ZnCl_2$ but with significantly increased quantities of C_8Im. None of these impurities were observed below the decomposition parameter $T_{1\%}$.

The decomposition product C_8Im is capable of coordinating metals through the nitrogen lone pair. Given the Lewis acidity of the chlorozincate ions, we next decided to spike $[C_8C_1Im]Cl_\chi ZnCl_2$ ionic liquids with 15 wt% C_8Im to probe potential interactions. Solution phase ^{1}H NMR showed that chemical shifts of C_8Im were shifted downfield in the presence of Lewis acidic $[C_8C_1Im]Cl_{0.6}ZnCl_2$ (ESI, Fig. S70 and Table S1†), supporting that coordination was occurring. Variable temperature NMR also suggested that this coordination was reversible and C_8Im could dissociate from the coordination complex (ESI, Table S2†). TGA analysis of the spiked C_8Im ionic liquid mixtures also proved to be insightful (Fig. 3f). The neutral C_8Im readily vaporised out of $[C_8C_1Im]Cl$ but was restricted from vaporising out of $[C_8C_1Im]Cl_{0.33}ZnCl_2$; however, it appeared that most of the C_8Im was lost before decomposition. Interestingly, $[C_8C_1Im]Cl_{0.6}ZnCl_2$ did not undergo any mass loss until complete thermal decomposition. This suggested that C_8Im was tightly bound to the Lewis acidic anion and consequently held in solution well beyond the boiling point of the neutral alkylimidazole. The C_8Im impurity was also observed to compromised thermal stability because decomposition started at a lower temperature than the pure ionic liquid.

Altogether, *ex situ* and *in situ* techniques demonstrated that imidazolium halometallate complexes were decomposing through similar mechanisms—chloride dissociation, followed by the reverse Menshutkin process, with the neutral *N*-alkylimidazolium products either vaporising or coordinating to Lewis acidic metals (Fig. 4). Previous work on *N*-methylimidazole complexes of palladium has shown that loss of methylimidazole during thermal decomposition produces three coordinate complexes that dimerise to give

Table 2 Positive mode ESI-MS data from *ex situ* analysis of TGA abort experiments

						Peak intensity				
Cation	Anion	Metal	χ	Temperature/°C	Mass decomposed/%	83	97	181	195	293
$[C_8C_1Im]^+$	Cl^-			180	0	0	0	0	100	0
				240	20	0	0.5	1.5	100	0.7
				263	60	0.1	1.9	3.5	100	11.8
$[C_8C_1Im]^+$	Cl^-	$ZnCl_2$	0.33	230	0	0	0	0	100	0
				316	20	0.3	1.6	7.1	100	2.1
				401	60	4.3	11.1	50.0	100	4.6
$[C_8C_1Im]^+$	Cl^-	$ZnCl_2$	0.6	334	0	0	0	0	100	0
				416	20	2.5	3.5	39.7	100	0.3
				471	60	4.5	8.6	61.8	100	1.0
$[C_8C_1Im]^+$	Br^-	$ZnBr_2$	0.33	396	60	1.7	2.8	62.9	100	4.1
$[C_8C_1Im]^+$	Cl^-	$NiCl_2$	0.33	375	60	2	1.2	100	65.2	13.2

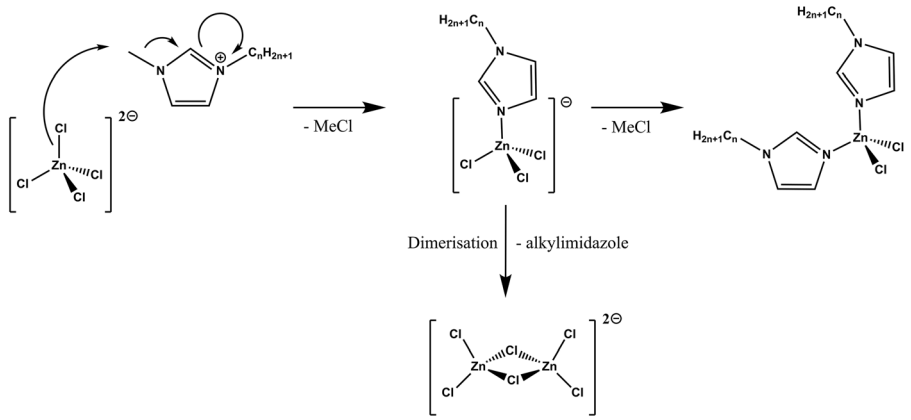

Fig. 4 Proposed scheme for thermal decomposition of halometallate ionic liquid in an inert N_2 atmosphere after $T_{1\%}$ (*e.g.*, >240 °C).

increasingly longer palladium chloride chains.[59] Dimerisation would explain the TGA profiles for the $[C_8C_1Im]Cl_\chi ZnCl_2$ series and support the observations of increasingly larger chlorozincate complexes at elevated temperatures. However, we cannot completely eliminate the formation of neutral complexes in competitive decomposition pathways.

To further support our experimentally measured data, we chose to calculate dissociation energies for chlorozincate complexes with DFT. In the gas phase, dissociation energies for loss of a single chloride anion from $[Zn_nCl_{2n+2}]^{2-}$ increased with larger amounts of Zn (Tables S3 and Fig. S137†), and thus calculations correlated with experimentally observed thermal stabilities. However, inclusion of a solvent continuum slightly affected this order, most notably for $[Zn_3Cl_8]^{2-}$ which readily dissociated through loss of Cl^- or loss of $ZnCl_2$ to give either $[Zn_3Cl_7]^-$ or $[Zn_2Cl_6]^{2-}$. While it was not clear why this particular chlorozincate complex was prone to dissociation in our calculations, experimental evidence supports the presence of $[Zn_3Cl_8]^{2-}$ in ionic liquids.[10] However, this discrepancy, along with the existence of other more unusual clusters observed in our calculations (Fig. S138†) in both the gas and solution phase, suggested that exotic structures may be accessed at elevated temperatures. Importantly, in all cases, $[Zn_4Cl_{10}]^{2-}$ was noted to be the most stable chlorozincate complex, which supported the experimentally measured high thermal stability of the ionic liquid. Interestingly, for $[ZnCl_4]^{2-}$ and $[Zn_2Cl_6]^{2-}$, the monoanionc dissociation products $[ZnCl_3]^-$ and $[Zn_2Cl_5]^-$ were more stable than the dicationic species in the gas phase, which supports previously observed mass spectrometry data for chlorozincate anions.[10] However, this trend is reversed with the addition of a continuum solvent environment, with $[ZnCl_4]^{2-}$ and $[Zn_2Cl_6]^{2-}$ being ~30 and 70 kJ mol^{-1} more stable than the monoanionic species.

To further probe the effects of different metal centres, activation energies (E_a) for thermal decomposition of the tetrahedral complexes (*i.e.*, $[ZnCl_4]^{2-}$, $[CoCl_4]^{2-}$ and $[NiCl_4]^{2-}$) with 1-alkyl-3-methylimidazolium cations were calculated using DFT. This method has previously been shown to provide qualitative estimates of the thermal decomposition temperatures of several ionic liquids.[60,61] Our results confirmed that the first decomposition step proceeds *via* a concerted SN2 reaction, similar to that found for $[C_4C_1Im][BF_4]$ ionic liquids.[61] At elevated temperatures, the volatile chloromethane product will rapidly vaporise from the solution, leaving the Lewis basic C_nIm and Lewis acidic MCl_3 which most likely form a Lewis pair. The E_a values calculated by DFT follow the experimentally observed TGA data: Ni (149.4 kJ mol^{-1}) > Co (148.8 kJ mol^{-1}) > Zn (147.8 kJ mol^{-1}). E_a values were comparable to those experimentally measured by TGA kinetics, but it must be considered that TGA E_a values are derived from the rate of mass loss which can capture multiple decomposition processes, rather than a single reaction. Despite this, DFT calculations supported the experimentally observed thermal stability trends and confirmed the hypothesised reaction mechanism.

3.3 Life cycle analysis

To further investigate the economic and environmental impacts of halometallate ionic liquid production, we decided to use a "cradle-to-gate" LCA approach. Production of ionic liquids is known to involve many steps because of their structural complexities,[5] and this was identified as a hotspot early on when compared to molecular solvents.[62] Thus, any benefits gained from ionic liquid use is offset by their production—burden shifting—which emphasizes that synthesis of ionic liquids is particularly problematic when scaling up. For this reason, protic ionic liquids have been identified as more sustainable alternatives because they are produced by acid–base neutralisation,[63] which avoids problematic steps such as alkylation and ion metathesis.[64] Although halometallate ionic liquids still require an alkylation reaction, their synthesis involves direct mixing of two components, as opposed to salt metathesis in solution. Halides are particularly problematic when looking at environmental impacts of ionic liquids.[64] However, with halometallate ionic liquids, halides are an integral part of the end product, and as the ratio of MCl_2 increases so does the halide content. Therefore, LCA analysis of halometallate ionic liquid can provide a valuable insight to production of the most industrially relevant ionic liquids.

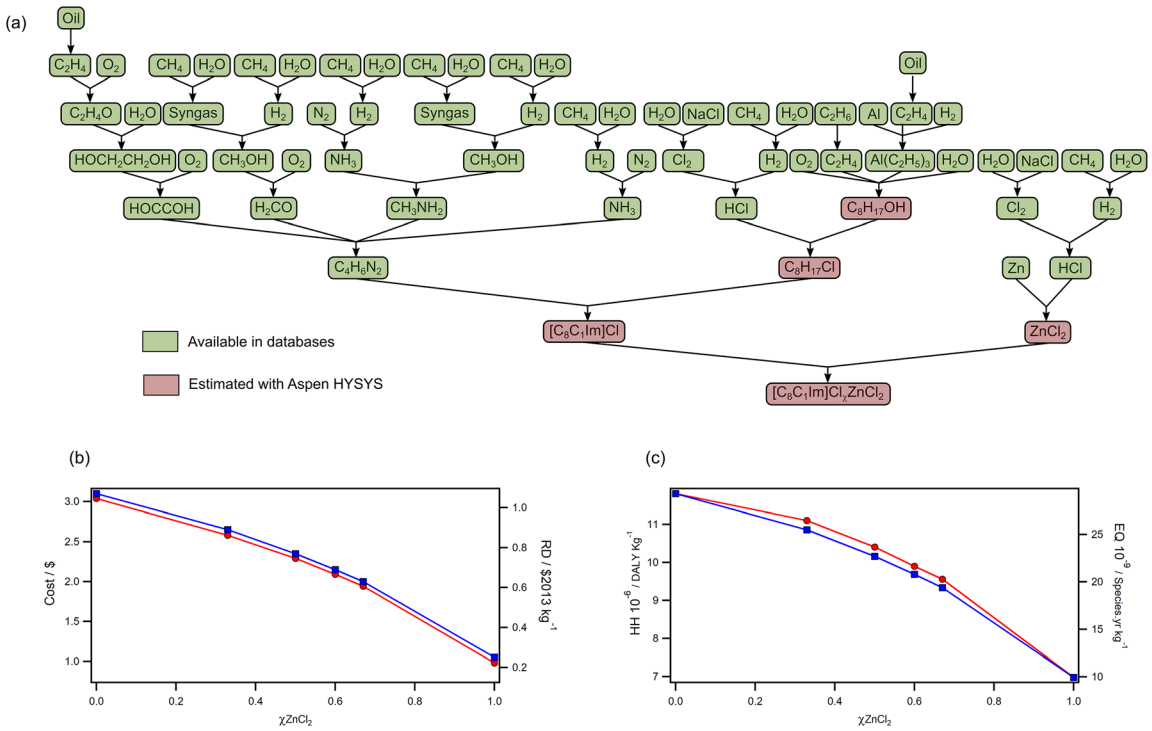

Fig. 5 (a) Lifecycle tree for $[C_8C_1Im]Cl_\chi ZnCl_2$ with lifecycle data for each mole fraction, showing (b) cost (left, red) and resource depletion (right, blue); (c) human health (left, red) and ecosystem quality (blue, right).

Here, we present LCA data for the chlorozincate $[C_8C_1Im]Cl_\chi ZnCl_2$ series as a case study to assess how the ratios of components affects environmental and economic impacts (Fig. 5). The lifecycle tree (Fig. 5a) highlights steps that were estimated with flow sheeting using Aspen HYSYS. Inspection of the tree shows that production of organic $[C_8C_1Im]Cl$ requires significantly more steps than production of inorganic $ZnCl_2$. Increasing quantities of $ZnCl_2$ therefore resulted in a significant decrease in cost and impact categories (Fig. 5b). For example, the cost of $[C_8C_1Im]Cl_{0.67}ZnCl_2$ was \$1.11 per kg lower than $[C_8C_1Im]Cl$, which is a 36% reduction. This is mainly due to the high cost of $[C_8C_1Im]Cl$ (\$3.04 per kg) compared to $ZnCl_2$ (\$0.97 per kg); $[C_8C_1Im]Cl$ is produced from 26 wt% 1–methylimidazole (\$2.84 per kg) and 74 wt% 1-chlorooctane (\$1.84 per kg), but $ZnCl_2$ is produced from 47 wt% Zn (\$1.66 per kg) and 53 wt% HCl (\$0.20 per kg).

The environmental impacts also decreased by similar percentages (EQ: 34%, RD: 41%) with the exception of human health (HH), which was reduced by 19% from that of $[C_8C_1Im]Cl$. This deviation reflects that the precursors for $ZnCl_2$ production are particularly problematic for human health (*e.g.*, Cl_2 and HCl), but overall, the decrease does support that fewer steps are inherently better. The decrease in resources depletion (RD) is primarily due to $[C_8C_1Im]Cl$; production of 1-chlorooctane and 1-methylimidazole are the main contributors at 68% and 28%, respectively. However, for $ZnCl_2$, the diethyl ether solvent used in production is the main contributor by 71%. Organic solvents can be replaced by better alternatives but starting materials cannot, so process development could further decrease the impact of high $ZnCl_2$ ionic liquids relative to non-metal counterparts. In the human health category, the main damage contributors for $[C_8C_1Im]Cl$ are again 1-chlorooctane and 1-methylimidazole by 69% and 21%, respectively, while Zn and $ZnCl_2$ are the main contributors for $ZnCl_2$ with 40% and 27% contributions, respectively. The contribution of $ZnCl_2$ is mainly due to air emissions of Zn and CO_2 from its production. Finally, the impact on ecosystem quality by $[C_8C_1Im]Cl$ is almost double that of $ZnCl_2$. For $[C_8C_1Im]Cl$, 1-chlorooctane and 1-methylimidazole contribute the most by 78% and 14%, respectively, while the main contributors in $ZnCl_2$ are $ZnCl_2$, Zn, diethyl ether and HCl (26%, 26%, 23% and 20% respectively). The results above show that only the precursors 1-chlorooctane and 1-methylimidazole are responsible for damages in all impact categories in $[C_8C_1Im]Cl$ while it varies by the damage area in the case of $ZnCl_2$ and it extends beyond precursors to include process emissions and solvents.

4. Conclusions

We have reported a wide range of industrially relevant thermal parameters for 26 halometallate ionic liquids, along with their metal-free analogues. Together, these parameters help define liquid ranges, provide a basis for estimating heating costs, and present upper temperature limits for processes. In terms of thermal stability, the identity of the metal centre had negli-

gible effects when compared to the identity of the ionic liquid cation or the mole fraction of the metal salt. These observations suggested that chloride dissociation was occurring during thermal decomposition, which was immediately followed by reverse Menshutkin chemistry in a concerted mechanism. TGA-MS and STA supported these observations, and *ex situ* analysis of decomposition residues showed that the neutral *N*-alkylimidazole by-products were forming Lewis adducts with halometallate anions. This was particularly problematic for highly Lewis acidic halometallate ionic liquids such as $[C_8C_1Im]Cl_{0.67}ZnCl_2$ because thermal stability was compromised by the change in speciation. Calculated M–Cl dissociation energies supported the observed stability trend for chlorozincate ionic liquids, but the presence of unusual clusters suggested that the inorganic ions could form more exotic structures at elevated temperatures.

Overall, our mechanistic insight provides a strong basis for designing more thermally robust halometallate ionic liquids to avoiding decomposition which will ultimately poison catalysts. Replacing or topping-up degraded solvents is environmentally damaging, especially when many steps are needed to meet the structural complexity inherent in ionic liquids. However, LCA calculations show that larger mole fractions of metals are better in terms of cost and environmental impact. This is largely due to the complexity of the organic cations, which has significantly more steps for production—simplicity is key. Theoretically, small amounts of $[C_8C_1Im]Cl$ could be used to lower melting points of molten salts into lower temperature regimes, bridging the gap between ionic liquids and molten salts. This would simultaneously reduce the economic and environmental impact of the medium, but physical and chemical properties must also be taken into consideration. This highlights that further work is needed to explore structure–property relationships in halometallate ionic liquids if they are to be successfully used on larger scales.

Author contributions

CJC conceived the project and carried out most of the experimental analysis. YC acquired TGA-MS and STA data, RPM carried out DFT calculations, and HB carried out life cycle analysis. The manuscript was written by CJC, RPM and HB and proof-read by all authors.

Conflicts of interest

There are no conflicts to declare.

Acknowledgements

CJC would like to thank Thomas Clayton (University of Nottingham), Istvan Matyi (TA Instruments), and Philip Davies (TA Instruments) for regular help and support with thermal analysis. JPH and CJC would like to thank EPSRC (EP/K038648/1) for financial support during the early stages of the project. PL and CJC would also like to thank EPSRC (EP/K005138/1 and EP/P013341/1) for support during the later stages of the project. KRJL acknowledges a Royal Society University Research Fellowship (URF\R\150353) for financial support, and RPM acknowledges support from a Daphne Jackson Fellowship – jointly funded by the Royal Society of Chemistry and the Royal Academy of Engineering. RPM also thanks the Imperial College Research Computing Service (**https://doi.org/10.14469/hpc/2232**) for computational resources.

Notes and references

1 K. Li, H. Choudhary and R. D. Rogers, *Curr. Opin. Green Sustainable Chem.*, 2018, **11**, 15–21.
2 A. J. Greer, J. Jacquemin and C. Hardacre, *Molecules*, 2020, **25**, 5207.
3 C. J. Clarke, W. C. Tu, O. Levers, A. Bröhl and J. P. Hallett, *Chem. Rev.*, 2018, **118**, 747–800.
4 F. Philippi and T. Welton, *Phys. Chem. Chem. Phys.*, 2021, **23**, 6993–7021.
5 P. G. Jessop, *Green Chem.*, 2011, **13**, 1391.
6 C. J. Clarke, S. Puttick, T. J. Sanderson, A. W. Taylor, R. A. Bourne, K. R. J. Lovelock and P. Licence, *Phys. Chem. Chem. Phys.*, 2018, **20**, 16786–16800.
7 C. J. Clarke, N. D. Richardson, A. E. J. Firth, J. P. Hallett and P. Licence, *ACS Sustainable Chem. Eng.*, 2020, **8**, 16386–16390.
8 F. Malaret, J. Hallett and K. S. Campbell, *Mater. Adv.*, 2020, **1**, 3597–3604.
9 C. J. Clarke, R. P. Matthews, A. P. S. Brogan and J. P. Hallett, *J. Mater. Chem. A*, 2021, **9**, 4679–4686.
10 J. Estager, P. Nockemann, K. R. Seddon, M. Swadźba-Kwaśny and S. Tyrrell, *Inorg. Chem.*, 2011, **50**, 5258–5271.
11 *Long chain halozincate anions can form three-dimensional chains of tetrahedral units in crystalline solids*: P. H. Fourcroy, D. Carré and J. Rivet, *Acta Crystallogr., Sect. B: Struct. Crystallogr. Cryst. Chem.*, 1978, **34**, 3160–3162.
12 J. Estager, J. D. Holbrey and M. Swadźba-Kwaśny, *Chem. Soc. Rev.*, 2014, **43**, 847–886.
13 J. Estager, A. A. Oliferenko, K. R. Seddon and M. Swadźba-Kwaśny, *Dalton Trans.*, 2010, **39**, 11375–11382.
14 M. Currie, J. Estager, P. Licence, S. Men, P. Nockemann, K. R. Seddon, M. Swadźba-Kwaśny and C. Terrade, *Inorg. Chem.*, 2013, **52**, 1710–1721.
15 A. W. Taylor, S. Men, C. J. Clarke and P. Licence, *RSC Adv.*, 2013, **3**, 9436.
16 F. Scé, I. Cano, C. Martin, G. Beobide, O. Castillo and I. De Pedro, *New J. Chem.*, 2019, **43**, 3476–3485.
17 Q. Wang, X. Lu, X. Zhou, M. Zhu, H. He and X. Zhang, *J. Appl. Polym. Sci.*, 2013, **129**, 3574–3581.
18 J. Zhou, L. Cheng and D. Wu, *e-Polym.*, 2011, **11**, DOI: **10.1515/epoly.2011.11.1.883**.
19 A. Chinnappan, A. H. Jadhav, H. Kim and W. J. Chung, *Chem. Eng. J.*, 2014, **237**, 95–100.

20 P. Filippousi, PhD thesis, Imperial College London, 2018.
21 C. J. Clarke, S. Hayama, A. Hawes, J. P. Hallett, T. W. Chamberlain, K. R. J. Lovelock and N. A. Besley, *J. Phys. Chem. A*, 2019, **123**, 9552–9559.
22 J. Seymour, E. Gousseva, A. Large, G. Held, D. Hein, G. Wartner, W. Quevedo, R. Seidel, C. Kolbeck, C. J. Clarke, R. Fogarty, R. Bourne, R. Bennett, R. Palgrave, P. A. Hunt and K. R. J. Lovelock, *Faraday Discuss.*, 2022, DOI: **10.1039/d1fd00117e**.
23 J. M. Seymour, E. Gousseva, A. I. Large, C. J. Clarke, P. Licence, R. M. Fogarty, D. A. Duncan, P. Ferrer, F. Venturini, R. A. Bennett, R. G. Palgrave and K. R. J. Lovelock, *Phys. Chem. Chem. Phys.*, 2021, **23**, 20957–20973.
24 V. Mamleev, S. Bourbigot, M. Le Bras and J. Lefebvre, *Three model-free methods for calculation of activation energy in TG*, 2004, vol. 78.
25 R. L. Blaine and B. K. Hahn, *J. Therm. Anal. Calorim.*, 1998, **54**, 695–704.
26 Y. Cao and T. Mu, *Ind. Eng. Chem. Res.*, 2014, **53**, 8651–8664.
27 C. J. Clarke, L. Bui-Le, J. P. Hallett and P. Licence, *ACS Sustainable Chem. Eng.*, 2020, **8**, 8762–8772.
28 M. T. Clough, K. Geyer, P. A. Hunt, J. Mertes and T. Welton, *Phys. Chem. Chem. Phys.*, 2013, **15**, 20480.
29 C. Xu and Z. Cheng, *Processes*, 2021, **9**, 337.
30 M. J. Frisch, G. W. Trucks, H. B. Schlegel, G. E. Scuseria, M. A. Robb, J. R. Cheeseman, G. Scalmani, V. Barone, G. A. Petersson, H. Nakatsuji, X. Li, M. Caricato, A. V. Marenich, J. Bloino, B. G. Janesko, R. Gomperts, B. Mennucci, H. P. Hratchian, J. V. Ortiz, A. F. Izmaylov, J. L. Sonnenberg, D. Williams-Young, F. Ding, F. Lipparini, F. Egidi, J. Goings, B. Peng, A. Petrone, T. Henderson, D. Ranasinghe, V. G. Zakrzewski, J. Gao, N. Rega, G. Zheng, W. Liang, M. Hada, M. Ehara, K. Toyota, R. Fukuda, J. Hasegawa, M. Ishida, T. Nakajima, Y. Honda, O. Kitao, H. Nakai, T. Vreven, K. Throssell, J. A. Montgomery, Jr., J. E. Peralta, F. Ogliaro, M. J. Bearpark, J. J. Heyd, E. N. Brothers, K. N. Kudin, V. N. Staroverov, T. A. Keith, R. Kobayashi, J. Normand, K. Raghavachari, A. P. Rendell, J. C. Burant, S. S. Iyengar, J. Tomasi, M. Cossi, J. M. Millam, M. Klene, C. Adamo, R. Cammi, J. W. Ochterski, R. L. Martin, K. Morokuma, O. Farkas, J. B. Foresman and D. J. Fox, *Gaussian 16 (Revision C01)*, Gaussian, Inc., Wallingford CT, 2016.
31 C. Lee, W. Yang and R. G. Parr, *Phys. Rev. B: Condens. Matter Mater. Phys.*, 1988, **37**, 785–789.
32 A. D. Becke, *J. Chem. Phys.*, 1993, **98**, 5648–5652.
33 J. P. Perdew, K. Burke and M. Ernzerhof, *Phys. Rev. Lett.*, 1996, **77**, 3865–3868.
34 J. Tao, J. P. Perdew, V. N. Staroverov and G. E. Scuseria, *Phys. Rev. Lett.*, 2003, **91**, 146401.
35 F. Weigend and R. Ahlrichs, *Phys. Chem. Chem. Phys.*, 2005, **7**, 3297–3305.
36 M. Cossi, N. Rega, G. Scalmani and V. Barone, *J. Comput. Chem.*, 2003, **24**, 669–681.
37 V. Barone and M. Cossi, *J. Phys. Chem. A*, 1998, **102**, 1995–2001.
38 R. Rowe, K. R. J. Lovelock and P. A. Hunt, *J. Chem. Phys.*, 2021, **155**, 014501.
39 G. Wernet, C. Bauer, B. Steubing, J. Reinhard, E. Moreno-Ruiz and B. Weidema, *Int. J. Life Cycle Assess.*, 2016, **21**, 1218–1230.
40 G. Towler and R. K. Sinnott, *Chemical Engineering Design - Principles, Practice and Economics of Plant and Process Design*, 2nd edn, 2013.
41 J. Estager, J. D. Holbrey and M. Swadźba-Kwaśny, *Chem. Soc. Rev.*, 2014, **43**, 847–886.
42 *Other competing thermal decomposition mechanisms can occur for electron donating anion, such as E2 Hofmann elimination*: M. T. Clough, K. Geyer, P. A. Hunt, J. Mertes and T. Welton, *Phys. Chem. Chem. Phys.*, 2013, **15**, 20480–20495.
43 K. R. J. Lovelock, J. P. Armstrong, P. Licence and R. G. Jones, *Phys. Chem. Chem. Phys.*, 2014, **16**, 1339–1353.
44 C. Deferm, A. Van Den Bossche, J. Luyten, H. Oosterhof, J. Fransaer and K. Binnemans, *Phys. Chem. Chem. Phys.*, 2018, **20**, 2444–2456.
45 H. L. Ngo, K. LeCompte, L. Hargens and A. B. McEwen, in *Thermochimica Acta*, Elsevier, 2000, vol. 357–358, pp. 97–102.
46 C. Li, Y. Wang, X. Guo, Z. Jiang, F. Jiang, W. Zhang, W. Zhang, H. Fu, H. Xu and G. Wu, *J. Phys. Chem. C*, 2014, **118**, 3140–3144.
47 Y. Shi, S. Bian, Y. Ma, Y. Wang, J. Ren and X. Kong, *J. Phys. Chem. A*, 2019, **123**, 187–193.
48 D. M. Calderón, U. Morales, C. Velásquez, V. H. Lara and L. Salgado, *Catal. Lett.*, 2009, **132**, 268–274.
49 S. Ichiba, S. Oshima, H. Negita and H. Tanaka, *Bull. Chem. Soc. Jpn.*, 1980, **53**, 3560–3562.
50 M. B. Meredith, C. H. McMillen, J. T. Goodman and T. P. Hanusa, *Polyhedron*, 2009, **28**, 2355–2358.
51 F. Jiang, H. Peng, C. Li, H. Fu and G. Wu, *Chin. Chem. Lett.*, 2020, **31**, 801–804.
52 M. B. Alves, A. P. Umpierre, V. O. Santos, V. C. D. Soares, J. Dupont, J. C. Rubim and P. A. Z. Suarez, *Thermochim. Acta*, 2010, **502**, 20–23.
53 Y. U. Paulechka, A. G. Kabo, A. V. Blokhin, G. J. Kabo and M. P. Shevelyova, *J. Chem. Eng. Data*, 2010, **55**, 2719–2724.
54 A. Diedrichs and J. Gmehling, *Fluid Phase Equilib.*, 2006, **244**, 68–77.
55 C. J. Clarke, P. J. Morgan, J. P. Hallett and P. Licence, *ACS Sustainable Chem. Eng.*, 2021, **9**, 6224–6234.
56 K. R. J. Lovelock, J. P. Armstrong, P. Licence and R. G. Jones, *Phys. Chem. Chem. Phys.*, 2014, **16**, 1339–1353.
57 M. Swadźba-Kwaśny, *RSC Adv.*, 2017, **7**, 51907–51909.
58 J. Wang, P. Zhou and H. Jing, *RSC Adv.*, 2017, **7**, 53686–53688.
59 M. C. N. Ranninger, M. G. Andrade and M. A. A. Franco, *J. Therm. Anal.*, 1978, **14**, 281–290.
60 S. D. Chambreau, A. C. Schenk, A. J. Sheppard, G. R. Yandek, G. L. Vaghjiani, J. Maciejewski, C. J. Koh,

A. Golan and S. R. Leone, *J. Phys. Chem. A*, 2014, **118**, 11119–11132.
61 M. C. Kroon, W. Buijs, C. J. Peters and G. J. Witkamp, *Thermochim. Acta*, 2007, **465**, 40–47.
62 Y. Zhang, B. R. Bakshi and E. S. Demessie, *Environ. Sci. Technol.*, 2008, **42**, 1724–1730.
63 H. Baaqel, I. Díaz, V. Tulus, B. Chachuat, G. Guillén-Gosálbez and J. P. Hallett, *Green Chem.*, 2020, **22**, 3132–3140.
64 H. Baaqel, J. P. Hallett, G. Guillén-Gosálbez and B. Chachuat, *ACS Sustainable Chem. Eng.*, 2022, **10**, 323–331.